



Research Article

Flexural behavior of concrete beams reinforced with glass fiber reinforced polymer and steel bars

Cristian Espíndola Farias¹, Sarah Lodeti Pessi², Augusto Wanderlind³, Jorge Henrique Piva^{4,*}, Elaine Guglielmi Pavei Antunes⁵

- ¹ Structural and Construction Performance Research Group, Department of Civil Engineering, University of the Southern Santa Catarina, Santa Catarina (Brazil), cristianfarias_ef@hotmail.com
- ² Structural and Construction Performance Research Group, Department of Civil Engineering, University of the Southern Santa Catarina, Santa Catarina (Brazil), sara.lodeti@hotmail.com
- ³ Structural and Construction Performance Research Group, Department of Civil Engineering, University of the Southern Santa Catarina, Santa Catarina (Brazil), acw@unesc.net
- ⁴ Structural and Construction Performance Research Group, Department of Civil Engineering, University of the Southern Santa Catarina, Santa Catarina (Brazil), jhpiva@gmail.com
- ⁵ Structural and Construction Performance Research Group, Department of Civil Engineering, University of the Southern Santa Catarina, Santa Catarina (Brazil), elainegpa@unesc.net

*Correspondence: jhpiva@gmail.com

Received: 31.03.2021; **Accepted:** 02.12.2022; **Published:** 29.12.2022

Citation: Farias, C., Pessi, S., Wanderlind, A., Piva, J. and Pavei, E. (2022). Flexural behavior of concrete beams reinforced with glass fiber reinforced polymer and steel bars. *Revista de la Construcción. Journal of Construction*, 21(3), 506-522. <https://doi.org/10.7764/RDLC.21.3.506>.

Abstract: In this study, a comparative experimental analysis is performed between steel-reinforced concrete beams, which are dimensioned based on NBR 6118 (2014), and beams reinforced with glass fiber-reinforced polymer (GFRP) rebar, which are dimensioned based on ACI 440.1R (2015) after being subjected to a four-point bending test. The beams are dimensioned to resist the same force and to satisfy the service limit state (SLS). Results show that the two groups of beams exhibit similar vertical displacement behaviors until the SLS-DEF, whereas the GFRP beams exhibit larger deflections. At the ultimate load, the beams with fiberglass bars indicate a higher resistance by approximately 64% compared with those with metal bars.

Keywords: concrete beams; fiber reinforced polymer; flexural strength; deflection.

1. Introduction

In conventional concrete structures, steel rebar's are used to complement the force exerted on the structural component, primarily via traction. The junction between concrete and steel results in durable and useful constructions because the steel is protected against corrosion by the alkalinity of the concrete. However, structures subjected to aggressive environments, such as marine structures, bridges, and parking lots exposed to defrosting salts and unfavorable humidity, temperature, and chlorides, may exhibit a reduction in concrete alkalinity and, consequently, steel corrosion. Corrosion ultimately results in concrete deterioration and structural weakening (ACI 2015).

Several methods for preventing steel corrosion have been investigated, including the replacement of steel with fiberglass-reinforced polymer bars (Umair-Saleem, Khurram, Nasir-Amin, & Khan, 2018). Owing to the advantages of glass fiber-

reinforced polymer (GFRP) composites, their application in specific structures such as bridges, viaducts, tunnels, deck slabs, reservoirs, among others, has expanded worldwide, and their characteristics have been further investigated (ACI, 2015).

According to American Concrete Institute (ACI) 440.1R (2015), GFRP bars can be regarded as a composite material with a high radius-to-length ratio that is suitable for the internal reinforcement of concrete. A GFRP bar comprises two elements: unidirectional glass fibers arranged longitudinally for the absorption of traction forces, and a polymeric matrix for protecting and transmitting tension between the fibers and the structure around them.

Concrete/steel adhesion can be improved by implementing helical ribs, and similar mechanisms can be employed in GFRP bars (Fava, Carvelli, & Pisani, 2016). According to Jabbar and Farid (2018) and Fava *et al.* (2016), the bond strength between concrete and GFRP bars is comparable to that of ribbed steel bars.

Compared with steel, GFRP is more advantageous, except for its properties. In particular, its lower modulus of elasticity results in larger deflections and cracks compared with conventional steel reinforced concrete structures (Yoo, Banthia, & Yoon, 2016b). The lower modulus of elasticity of GFRP can adversely affect the shear strength of beams constructed using it (Sheikh & Kharal, 2018; Yoo, Banthia, & Yoon, 2016a). According to ACI 440.1R (ACI, 2015), (Ascione, Mancusi, & Spadea, 2010; El-Nemr, Ahmed, El-Safty, & Benmokrane, 2018), GFRP bars do not flow and behave linearly elastic until failure. Consequently, the dimensions of these structures are governed by the service limit states of vertical movement and crack widths. Owing to the low modulus of elasticity, concrete members reinforced with fiber-reinforced polymer (FRP) bars undergo large deflections and wider cracks, which affect their serviceability. Recently, researchers have reported the combination of steel bars with FRP bars (hybrid system) for reinforcing concrete structures, which overcomes the ductility and serviceability issues of purely FRP-reinforced structures (Ramachandra Murthy, Pukazhendhi, Vishnuvardhan, Saravanan, & Gandhi, 2020).

Several studies have resulted in the development of standards for concrete structures reinforced with FRP bars (Saleh, Goldston, Remennikov, & Sheikh, 2019), including the “Guide for the Design and Construction of Concrete Structures Reinforced with Fiber-Reinforced Polymer Bars (FRP)” (ACI, 2015) and the “Design and Construction of Building Structures with Polymer-Reinforced Fibers” (CSA S806, 2012). However, research addressing code recommendations for the bending design of GFRP-reinforced concrete beams is inadequate compared with experimental results performed based the Brazilian standard.

Therefore, this study is performed to experimentally analyze and compare the behavior of concrete beams reinforced with steel rebars sized based on ABNT NBR 6118 (2014), with that of concrete beams reinforced with GFRP bars sized based on ACI 440.1R (2015), via four-point bending tests. Beams exhibiting equivalent dimensions that can resist the same bending moment are used, while considering the limit state of excessive deformation.

2. Materials and experimental program

To achieve the objective of this study, two beam groups were established; both were fabricated using conventional concrete, with differences in the longitudinal reinforcements in terms of the material type, diameter in the coverings, and stirrup spacing. The first group, abbreviated REF, refers to beams fully reinforced with steel rebars, and the second group, abbreviated as GFRP, refers to beams longitudinally reinforced with GFRP bars and transversally reinforced with steel. The two groups exhibited the same dimensions, i.e., 210 cm long, 15 cm wide, and 25 cm high. Three beams were used for each group.

In the REF group, as longitudinal reinforced concrete measuring $2 \phi 8$ mm was used, which was equivalent to a steel area of 1 cm^2 . The transverse reinforcement was dimensioned by adopting the I model of calculation, with stirrups implemented in the vertical direction ($\alpha = 90^\circ$). The REF group was dimensioned based on a structure exposed to tidal splashes, classified based on NBR ABNT 6118 (2014) with class-IV environmental aggressiveness. Subsequently, a nominal reinforcement cover measuring 50 mm as well as concrete with a characteristic resistance to compression greater than or equal to 40 MPa were

used. However, considering the environmental conditions, 30 MPa was adopted because of the greater ease of technological control over concrete.

For laboratory analysis, all the load weighting coefficients (increase) or material resistance (decrease) were assumed to be 1, which implies that all the resisted or desired loads exhibited characteristic values. To calculate the resistance efforts of the REF beam group, the values based on the specifications of steel listed in Table 1 were adopted.

Table 1. Characteristics of steel rebars (source: supplier, 2018).

Feature	Units	Reinforced concrete	Stirrup holders and stirrups
Nominal diameter	mm	8	5
Section Area	cm ²	0,50	0,20
Category	-	CA-50	CA-60
Characteristic resistance (Fyk)	MPa	500	600
Modulus of elasticity (Es)	MPa	210000	210000
Surface	-	Nervured	Nervured

Based on the characteristics of the cross-section of the beam and the materials used, longitudinal reinforced concrete measuring 2 ϕ 8 mm, stirrups measuring 2 ϕ 5 mm, and stirrups measuring ϕ 5 mm every 11 cm were used in the REF group. The section was framed in deformation domain 2, with an x/d ratio of 0,0860. Therefore, the REF beam can, by dimensioning, withstand a characteristic bending moment $M_k = 9,1732 \text{ kN}\cdot\text{m}$. The loads applied in the bending test at four points to obtain the bending moment are shown in Figure 1. The loads from the weights of the beams were disregarded.

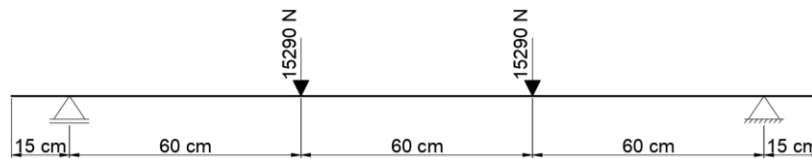


Figure 1. Loads considered in the beams.

The GFRP rebar used was a composite composed of two materials, i.e., fiberglass, whose characteristics are listed in Table 2, and an epoxy ester-vinyl resin of bisphenol, whose mechanical properties are listed in Table 3.

Table 2. Mechanical properties of glass fiber (source: supplier, 2019).

Properties	Units	-	Test method
Type of glass	-	Glass E (corrosion resistant)	-
Tex (linear mass)	g/km	8800	-
Average diameter of the filament	μm	33,00	-
Tensile strength with the use of epoxy resin	MPa	2700,00	ASTM D 2343
Tensile strength using polyester resin	MPa	2570,00	ASTM D 2343

Table 3. Mechanical properties of resin (source: supplier, 2019).

Properties at 25°C	Unit	1/8" transparent casting	Test method
Resistance to bending	MPa	158,60	ASTM D 790
Tensile strength	MPa	80,00	ASTM D 638
Elastic elongation (at break)	%	5,20	ASTM D 638
Thermal deflection temperature	°C	104,40	ASTM D 648

Finally, rebars with properties expressed in Table 4 and dimensions as shown in Figure 2 were achieved. Figure 2 (a) presents a top view of the bar and (b) a microscopic view of the cross-section.

Table 4. GFRP rebar characteristics (source: supplier, 2018).

Feature	Units	Reinforced concrete	Stirrup holders
Nominal diameter	mm	12,50	6,20
Section area	mm ²	125,00	29,80
Density	kg/m ³	2200,00	2200,00
Medium tensile strength	MPa	989,00 ± 93,90	1015,00 ± 96,40
Modulus of elasticity	MPa	48000,00	48000,00
Poisson coefficient	-	0,26	0,25
Stretching	%	2,05	2,12
Longitudinal thermal expansion coefficient	× 10 ⁻⁶ /°C	5,90	5,90
Transverse coefficient of thermal expansion	× 10 ⁻⁶ /°C	28,70	27,30
Moisture absorption	%	0,43	0,65

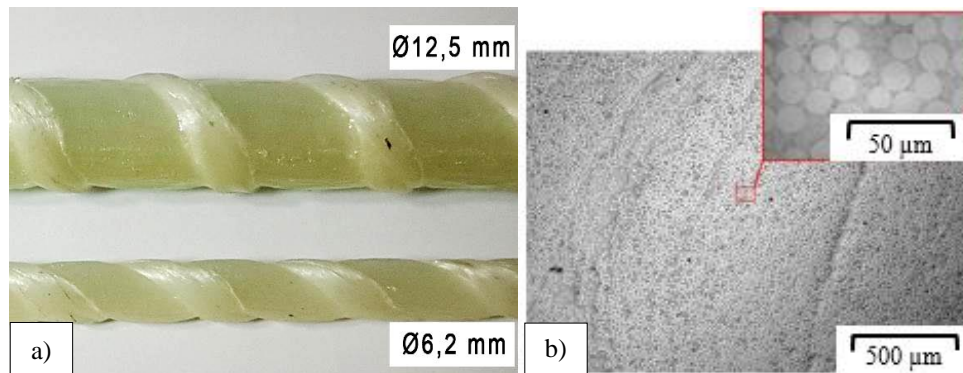


Figure 2. GFRP rebars: (a) exterior dimensions; b) cross-section microscopy image.

After the desired resistances of the materials and the effects from the loads resisted by the REF group were achieved, the beams of the GFRP group were sized based on the criteria of ACI 440.1R (2015). In this regard, the beam dimensions were preserved, and the rebar repositioning, as established by ACI 440.5 (2008), resulted in a height (*d*) of 193 mm. This standard establishes the nominal cover of the minimum GFRP reinforcement for beams, i.e., 38 and 50 mm for stirrups and longitudinal reinforcement, respectively. The calculation sequence for this step is presented in Table 5.

Table 5. Bending strength dimensioning of GFRP group based on ACI 440.1R.

Calculated item	Remarks	Equation used [2]	Result obtained
Guaranteed rebar tensile strength (f_{tu}')	Obtained by calculating the average resistance minus three times the standard deviation of the rebars.	-	$f_{tu}' = 707,00$ MPa
Rebar calculation tensile strength (f_{tu})	Minimized value used for all dimensioning. Value obtained from the product between f_{tu}' and a reduction factor, CE (CE = 0,70**).	Eq. (6.2a)	$f_{tu} = 707,00$ MPa
Rebar reinforcement rates	The relationship between the reinforcement rate (ρ_f) and the balanced reinforcement rate (ρ_{fb}) reveals the material, i.e., either concrete or GFRP, that is the most susceptible to	ρ_f is obtained using Eq. (7.2.1a); ρ_{fb} is	$\rho_f = 0,00864$

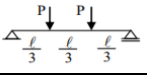
	breakage. When $\rho_f < \rho_{fb}$, the section is controlled by the rebar breakage; otherwise, it is controlled by the crushing of the concrete.	obtained using Eq. (7.2.1b)	$\rho_{fb} = 0,00488$
Nominal bending strength (Mn)	Nominal bending moment that the beam can withstand. The calculation varies depending on the relationship between ρ_f and ρ_{fb} .	Eq. (7.2.2e)	$M_n = 22,70 \text{ kN}\cdot\text{m}$

** Minority factors were assumed to be 1 for this survey

The use of $2 \phi 12,5 \text{ mm}$, which was equivalent to a bending reinforcement area of 250 mm^2 , proved to be sufficient for the absorption of the requested efforts.

Despite the oversizing of the GFRP beams to the ultimate limit state based on a comparison between the desired bending moment and the resistor, the limiting factors that must be prioritized in this type of structure are directly related to the service limit states (SLS) because the low modulus of elasticity of the rebars results in greater vertical displacements in the beams. This is the most critical aspect in dimensioning, as specified by ACI 440.1R (ACI (2015)). The calculation of the immediate deflection is presented in Table 6.

Table 6. Sizing for immediate deflection control.

Calculated item	Remarks	Equation used based on ACI 440.1R	Result obtained
Critical crack moment (Mr)	Bending moment of service at which the section tends to crack.	Eq. (7.3.2.2d)	$M_r = 5,31 \text{ kN}\cdot\text{m}$
Effective moment of inertia of the section (Ie)	When $M_{sk} > M_r$, the section is in deformation stage II; this is considered in the effective moment of inertia.	Eq. (7.3.2.2c)	$I_e = 2228 \text{ cm}^4$
Concrete drying modulus of elasticity (Ecs)	Calculated based on Section 8.2.8 of ABNT NBR 6118 [1].	-	$E_{cs} = 26838 \text{ MPa}$
Section characteristics and loads required for sizing	Effective beam span, $L = 1800 \text{ mm}$; point load, $P = 15290 \text{ N}$	-	-
Immediate deflection		$f = \frac{23 * P * L^3}{648 * E_{cs} * I_e}$	$f = 5,29 \text{ mm}$
Boundary deflection	$f_{max} = \frac{L}{250}$	-	$f_{max} = 7,20 \text{ mm}$

By adopting a vertical displacement limit of $L/250$, as stipulated in NBR ABNT 6118 (2014), the deformation limit of the structure owing to sensorial and visual issues satisfied the requirements of the standard. In the experimental tests, only the immediate deflection was evaluated. When durable structures are used, the deferred deflection must be verified timely.

As the bending resistance of the samples was primarily analyzed, steel stirrups were used in the GFRP group to accelerate the production of rebars, as the process of bending fiberglass bars is more time consuming.

Nevertheless, considering the use of the GFRP stirrups, the spacing of the stirrups was calculated based on ACI 440.1R (2015). In this regard, the properties of the rebars (ϕ 6,20 mm, as shown in Table 4) must be used. Table 7 summarizes the dimensions of the transverse reinforcement used.

Table 7. Sizing of transverse reinforcement.

Calculated item	Remarks	Equation used based on ACI 440.1R	Result obtained
Guaranteed rebar tensile strength (f_{tu}')	Obtained by calculating the average resistance minus three times the standard deviation of the rebars.	-	$f_{tu}' = 725,00$ MPa
Rebar calculation tensile strength (f_{tu})	Minimized value used for all dimensioning. Value obtained from the product between f_{tu}' and a reduction factor, CE (CE = 0,70**).	Eq. (6.2a)	$f_{tu} = 725,00$ MPa
Shear strength provided by concrete (ϕV_c)	Concrete's contribution to shear strength, reduced by a factor $\phi = 0,75$ **.	Eq. (8.2a)	$\phi V_c = 10,21$ kN
Verifying the necessity for transverse reinforcement	If the maximum characteristic cutting effort exceeds $\phi V_c/2$, then transverse reinforcement is required; otherwise, it is not.	$V_{sk} = 15,29$ kN > $\phi V_c/2 = 5,11$ kN	The use of stirrups is necessary
GFRP reinforcement area ($A_{fv,nec}$)	Area required to supply the cutting effort.	Eq. (8.2e)	$A_{fv,nec} = 0,1371$ mm ² /mm
Maximum spacing between stirrups	Resulting from $A_{fv,nec}$. Considering two branches of stirrups, $A_{fv} = 59,6$ mm ²	$S = \frac{A_{fv}}{A_{fv,nec}} = \frac{59,60}{0,1371}$	$S = 434$ mm
	Result obtained from verifications based on ACI 318 [13] and the useful height (d) of the beam.	$S = \frac{d}{2} \leq 600$ mm	$S = 96$ mm
	Maximum spacing based on the minimum shear armor	Eq. (8.2.2)	$S = 218$ mm
Spacing adopted between stirrups	The lowest calculated value is adopted, rounded to whole numbers.	-	$S_{m\acute{a}x} = 90$ mm

** Minority factors were assumed to be 1 for this survey

Therefore, the sizing of the transversal reinforcement of the GFRP beams, which was executed using metal rebars measuring ϕ 5 mm, resulted in stirrups every 9 cm.

The final details of the REF and GFRP groups are shown in Figure 3, which illustrates the cross-section of the beams and reinforcement coverings. Meanwhile, Figures 4 and 5 show the details of the models used.

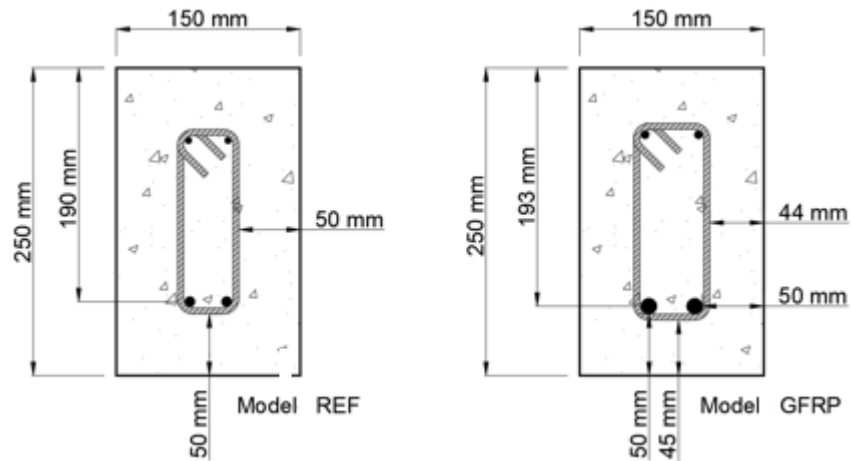


Figure 3. Cross-section of the analyzed models.

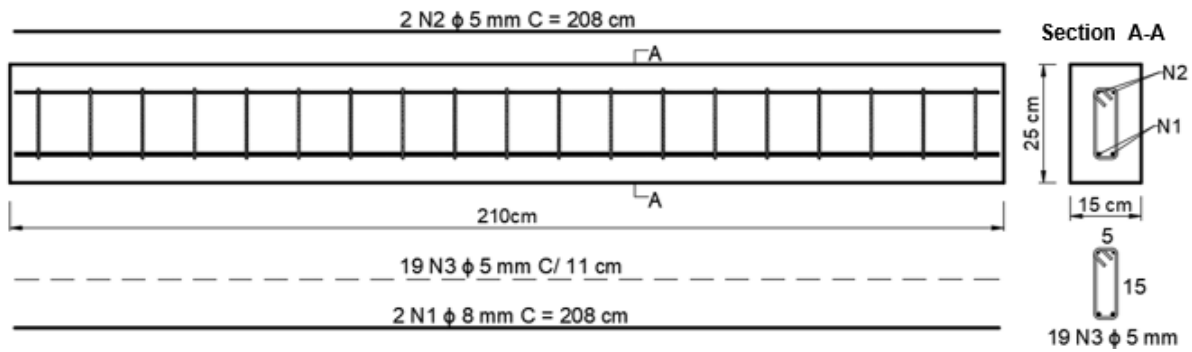


Figure 4. Details of the REF beam.

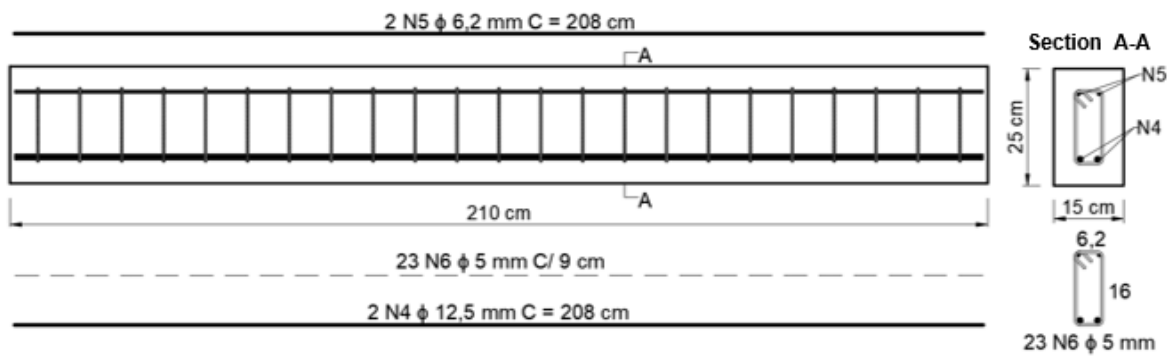


Figure 5. Details of the GFRP beam.

Strain gauges were inserted into the center of the span in one of the bars that comprised the longitudinal reinforcement in all the beams of both groups. The details of the strain gauge installation are shown in Figure 6. The final result of the reinforcement is shown in Figure 7.

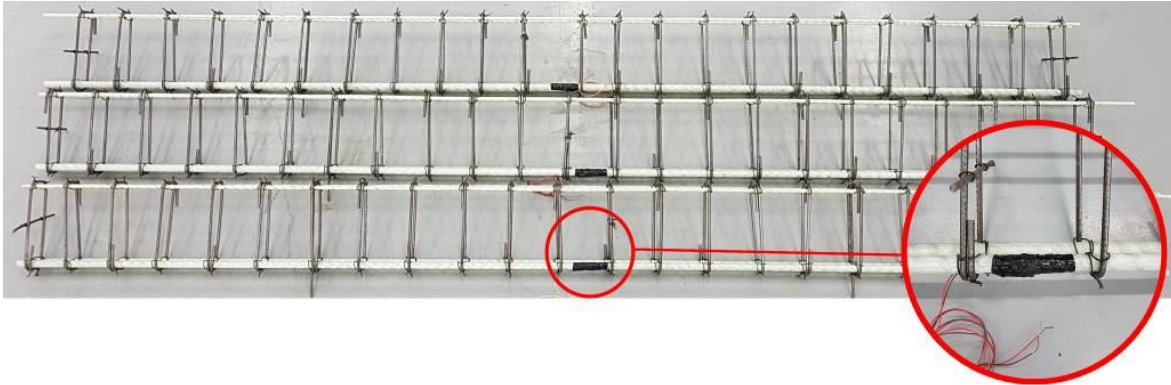


Figure 6. Details of strain gauges installed in the GFRP beams.

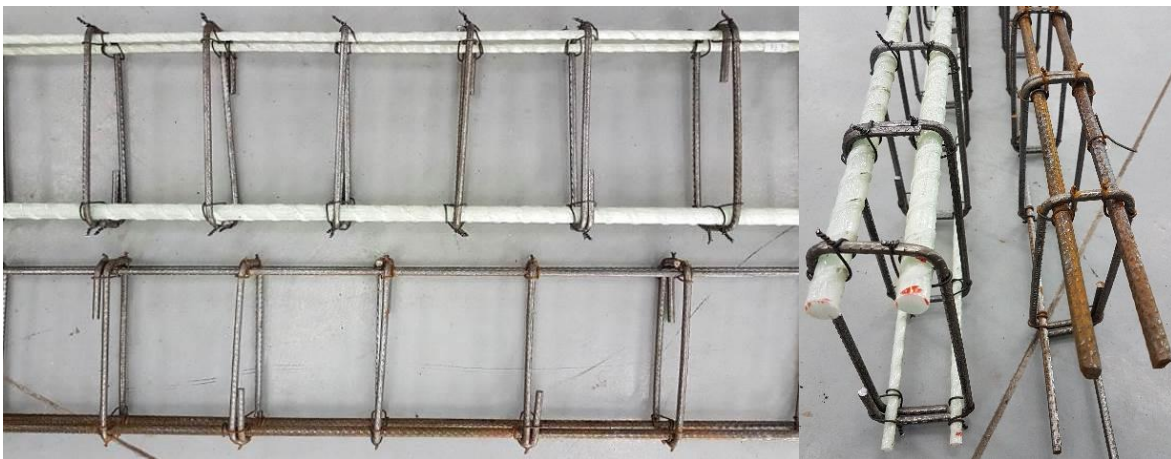


Figure 7. Details of steel reinforcements and GFRP used.

The concrete used was fabricated in the Laboratory of Building Materials of the UNESC (University of the Southern Santa Catarina), and the trace used was based on Hoffman and Antunes (2017). The characteristics of the concrete used are listed in Table 8.

Table 8. Trace and properties of concrete used.

Mass unitary trace	1:2,87:2,13
Water/cement ratio	0,48
Cone trunk closure	50 mm

Table 9 presents the characteristics of the aggregates used to fabricate the concrete, whose characterization was performed based on ABNT NBR NM 248 (2003).

Table 9. Properties of aggregates used in concrete (source: laboratory of building materials of UNESC, 2017).

Aggregate	Medium-washed sand	Gravel 3/4
Fineness modulus	2,37	6,65
Maximum characteristic dimension	2,40 mm	19,00 mm
Mineralogical composition	Quartz	Basalt
Specific dry mass (kg/m ³)	2364,91	2999,06
Unit mass (kg/m ³)	1580,70	1542,98

The formwork used for the beams was constructed using *Pinus elliottii* wooden boards. A wire and metallic rebars were tied to the formwork to accommodate the cover of the concrete reinforcement. Figure 8 shows the group of REF concrete beams and the GFRP group ready for concreting.



Figure 8. REF beams and GFRP beams assembled before concreting.

Four cylindrical specimens (10 cm × 20 cm) of concrete were used for each beam group (based on the guidelines of ABNT NBR 5738 (2015)), cured in water with calcium hydroxide solution, and ruptured using a hydraulic press model (Emic SSH300) at 28 d, based on the procedures stipulated in ABNT NBR 5739 (2018).

After concreting and curing for 28 d, all beams were subjected to destructive experiments at UNESC's Experimental Laboratory of Structures using an HBM U10M load cell with a 500 kN capacity. Four-point bending tests were performed in these experiments based on the scheme shown in Figure 9. The tests were performed based on the orientation specified in ASTM C78 (2018), with adaptations to the height of the beam and the geometry of the support mechanisms. To obtain the vertical displacement values, two LVDTs positioned at the center of the span, i.e., one on each side of the beam, were used.

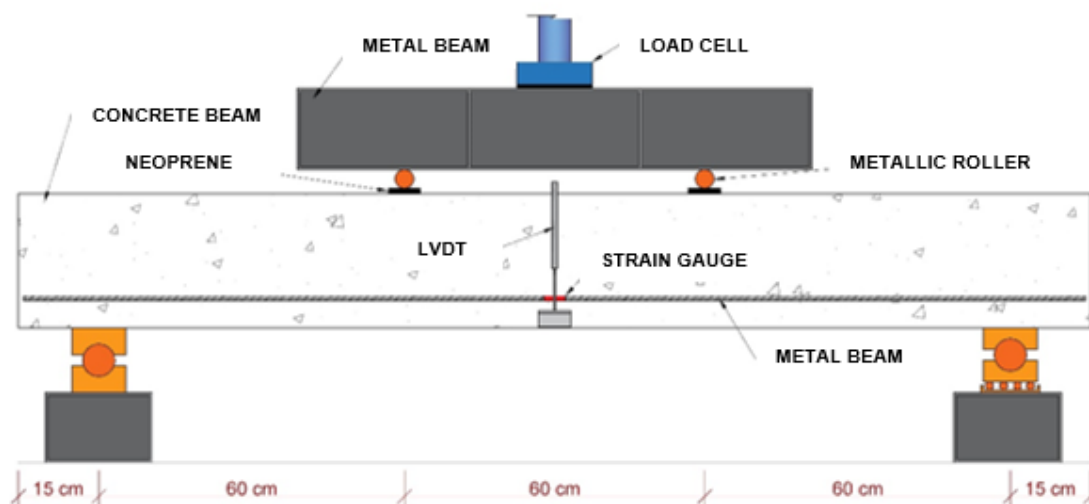


Figure 9. Illustration of setup for four-point bending test.

The overall response of the specimens analyzed during and after the four-point bending test was evaluated in terms of the load capacity, maximum vertical displacement at the center of the span, deformation of the reinforced concrete, and failure mode of the beams.

3. Experimental results and analysis

The concrete used in the REF group achieved a mean axial compressive strength of $33,57 \pm 1,03$ MPa whereas that in the GFRP group achieved $30,55 \pm 0,59$ MPa. The results show that the concrete used in this study yielded the desired resistance.

The images of ruptured beams of the two groups are shown in Figure 10. For a better visualization, the cracks that appeared during load application are mapped, and the positions of the loads and supports are shown. The yellow arrows indicate the center of the aperture, and the red arrows indicate the locations of the load.

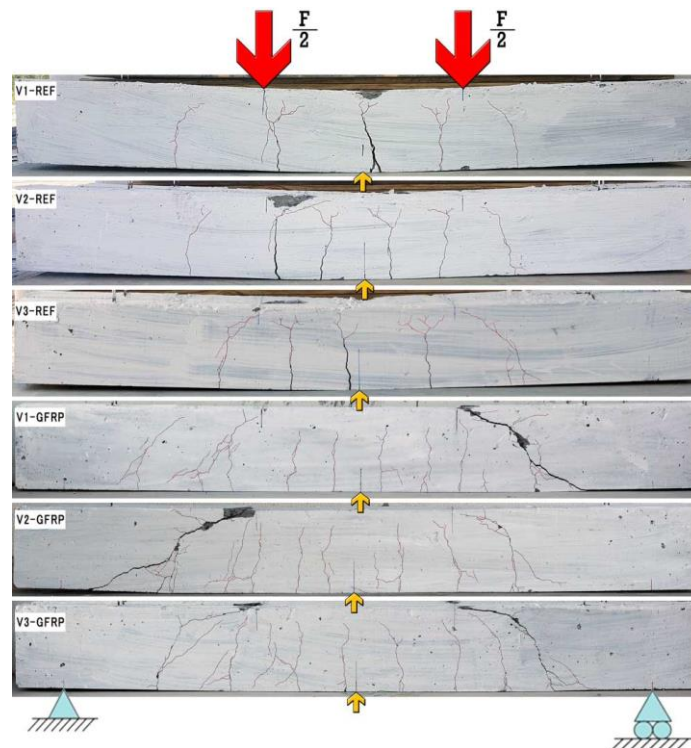


Figure 10. Condition of samples after test.

Based on the mapping of cracks shown in Figure 10, the number of openings in the GFRP group was significantly higher than that in the REF group. Tavares and Giongo (2009) observed similar behaviors in their study, in which they attributed the more ductile characteristic of the beams to the low modulus of elasticity of fiberglass bars. Similarly, differences were observed in terms of the development of cracks in the central regions of the beams in both groups. In the GFRP group, the beams propagated vertically with few cracks, whereas in the REF group, cracks appeared in the compressed section of the beams, which is likely caused by the high crushing tension in the concrete.

In addition, as shown in Figure 10, a more accentuated residual curvature (deflection) was observed in the REF beams, which indicates that the metal concrete reinforcement may have entered the plastic deformation state because the cracks due to bending remained opened after the load was removed. Because the GFRP rebar exhibited an elastic linear behavior until failure, when the load was interrupted, the beam returned almost completely to the initial state of linearity, and the bending openings were closed.

Based on the visualized cracks and crevices, the GFRP beams presented sloping cracks in the central zone that originated from shearing forces, which was not observed in the REF group. Notably, these shear cracks began to appear in the GFRP-reinforced beams when a load of approximately 60 kN was exerted, i.e., a magnitude that could not be supported by the steel-reinforced beams.

In the REF group, the rupture of the samples was caused by the possible flow of steel followed by the crushing of concrete. Meanwhile, in the GFRP group, the three beams failed via shearing and resulted in a fracture in the armature of the stirrups holder in the direction of crack in specimens V1-GFRP and V2-GFRP, as illustrated in Figure 11.



Figure 11. Fractured split holder of V1-GFRP.

The concrete/rebar connection, evaluated visually in the bending armature at the center of the span, was shown to be complete. The surrounding concrete adhered firmly to the metal and GFRP bars at the evaluated point, as presented in Figure 12, where the (a) concrete/GFRP bond and (b) concrete/steel bond are shown.

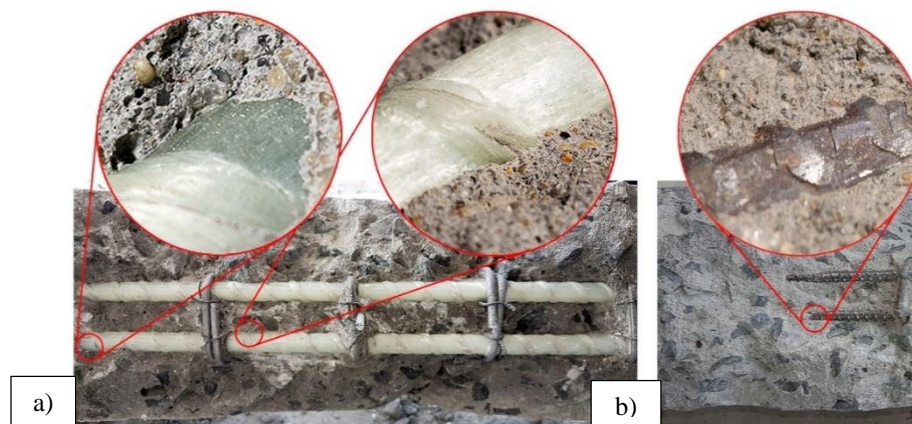


Figure 12. Details of the concrete/rebar connection: (a) concrete/GFRP bond; (b) concrete/steel bond.

Fava *et al.* (2016) performed pulling tests and concluded that the adherence of metallic and polymeric reinforcements to concrete exhibited similar strengths, although the failure mode of GFRP reinforcements was caused by the peeling of the rebar, whereas that of metallic reinforcements was the rupture of the surrounding concrete. As expected, the adhesion between the concrete and reinforcement materials did not result in any type of failure.

Figure 13 shows the maximum resisted moments in each group and their respective characteristic values for performing calculations, based on the guidelines stipulated in the relevant standards.

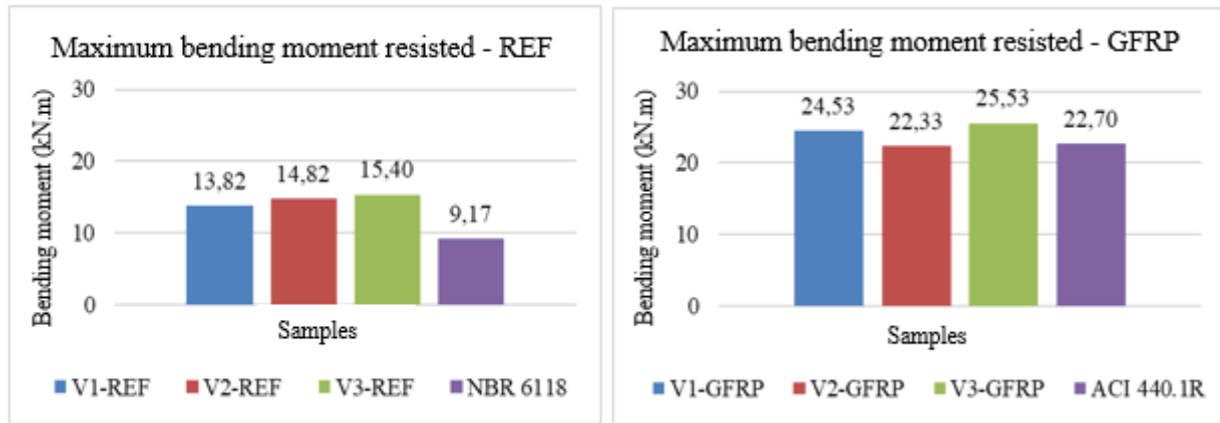


Figure 13. Maximum bending moments resisted.

Although dimensioned to resist the same force, the fiberglass rebars (whose modulus of elasticity is low), demanded a greater area of reinforcement to accommodate bending in the structure to satisfy the SLS. Thus, the different reinforcement areas between the two groups resulted different maximum resistance moments. The beams of the GFRP group withstood a load of $24,13 \pm 1,337$ kN·m, which was approximately 64% higher than that withstood by the beams reinforced with metal rebars, as expected.

The results show that the dimensioning of the GFRP beams based on the maximum bending moment characteristics stipulated in ACI 440.1R (2015) resulted in values that were similar to those obtained in the tests. Only one of the samples, V2-GFRP, disintegrated earlier than expected, but did not alter the result significantly. This was similarly reported by Abdelkarim *et al.* (2019), who achieved similar results with a difference of $\pm 2\%$ between the maximum bending moment calculated and that verified via tests. Meanwhile, Confrere *et al.* (2016) divided the calculated maximum bending moment by the average maximum resistance and obtained a value of 0,83. However, in the current study, a ratio of 0,94 was obtained, i.e., the forecast by ACI 440.1R (2015) was similar to the experimental result.

Meanwhile, Figure 13 shows that the maximum bending moments resisted by the REF beams, i.e., $14,68 \pm 0,653$ kN.m, resulted in values that were 60% higher on average compared with those calculated based on NBR 6118 (2014), indicating an underestimation of resistance calculation in favor of safety.

The analysis of the specific deformations of the two groups based on measurements obtained using the strain gauges is shown in Figure 14.

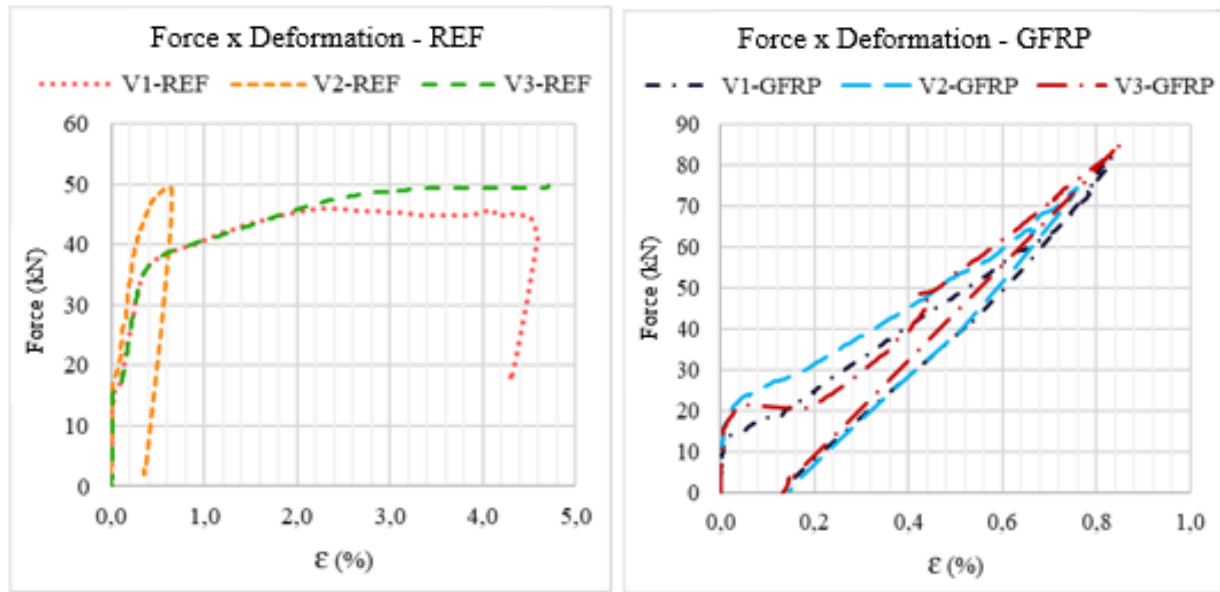


Figure 14. Force vs. deformation.

As shown in Figure 14, the ultimate stress was achieved via strengthening using steel bars (REF), which implies the failure of beams V1-REF and V3-REF via reinforcement plasticization. However, in beam V2-REF, this behavior did not occur, and no cracks appeared in the tensioned region; therefore, the beam showed damage in the compressed region of the concrete.

An analysis of the strain levels of the GFRP-strengthened beams showed that their maximum longitudinal strain was lower than their total capacity. In fact, this property is necessary to avoid excessive vertical deformation on the beam caused by the low modulus of elasticity of the GFRP. Thus, the failure of the beams strengthened with GFRP evolved from concrete rupture to compression, which did not place a high demand for tensile reinforcements.

Figure 15 presents the force vs. vertical displacement graphs for all tested beams. The point of excessive deformation limit state (SLS-DEF), which was $L/250$ for this study, resulted in a 7,20 mm deflection; it is indicated on the graph for a better visualization of the behavior of the beams.

The behavior of the beams of the two groups can be compared based on Figure 15. Initially, in deformation stage I, both units tested showed similar behaviors since in this stage, the concrete had not yet cracked and the reinforcement had not been requested. The demarcation between deformation stages I and II (at approximately 15 kN) is clearly indicated in the graph. In stage II, where cracks occurred, the concrete no longer contributed completely to the tensile strength of the reinforced concrete structures (Filho, 2014); therefore, the bending reinforcements began to function as intended. The behavior of the analyzed beams changed once cracking occurred. In the SLS, the REF beams showed high resistance. They supported higher loads and demonstrated smaller deflections compared with the GFRP armed beams.

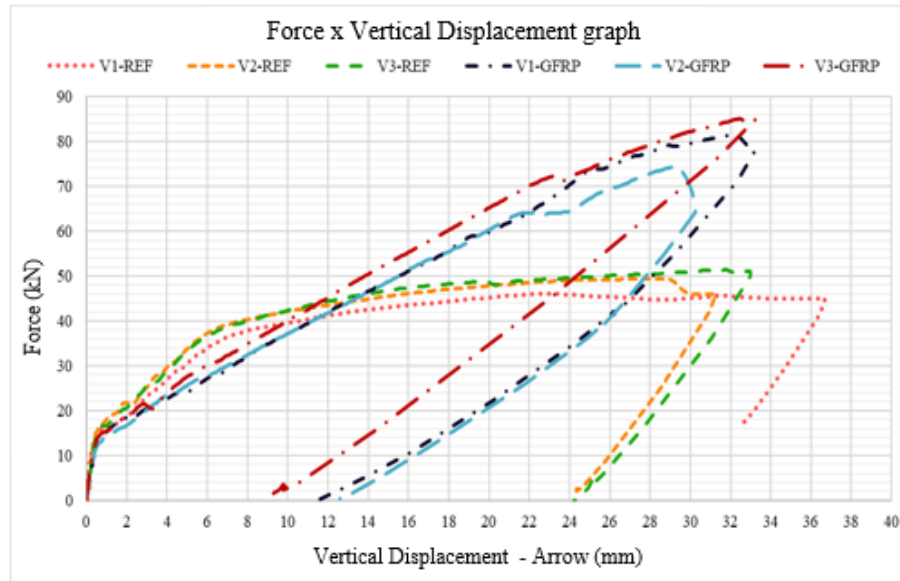


Figure 15. Force vs. vertical displacement.

The $L/250$ limit deflection was attained by the GFRP group at an average load of $31,08 \pm 1,221$ kN, whereas the REF group attained it at $38,37 \pm 1,170$ kN, which was approximately 23% higher than that supported by the GFRP beams. After the maximum deflection, the GFRP group resisted an increase of approximately 160% of the load until rupture, whereas the steel beams exhibited an increase of approximately 30%.

The experimental deflections that yielded the desired bending moment, $M_k = 9,1732$ kN·m, in the beams of the REF and GFRP groups were $4,55 \pm 0,326$ and $6,95 \pm 0,550$ mm, respectively. Whereas the steel-reinforced beams functioned as intended inside the SLS-DEF, the two beams of the GFRP group exceeded the maximum vertical movement.

When a force of approximately 38 kN was applied, the bending force vs. displacement of the steel-reinforced beams began to bend horizontally, which resulted in greater deflections with lower loads, possibly due to the flow of the rebars. Beginning from approximately 42 kN, owing to the linear deformation of the GFRP reinforced beams, an opposite scenario was observed. The GFRP beams was able to withstand an increase in load by approximately 90%, whereas the steel-reinforced beams withstood only a load of 17% until rupture. Notably, the average maximum deflections yielded by groups REF and GFRP were $33,67 \pm 2,270$ and $32,24 \pm 1,413$ mm, respectively. Additionally, based on the results of the analysis of variance with 95% reliability, the maximum displacement between the beams of the two groups did not show any statistical difference.

By analyzing the immediate theoretical vertical displacements of the beams based on the calculation criteria suggested by each norm and then comparing these results with the experimental results, the graphs shown in Figure 16 were obtained.

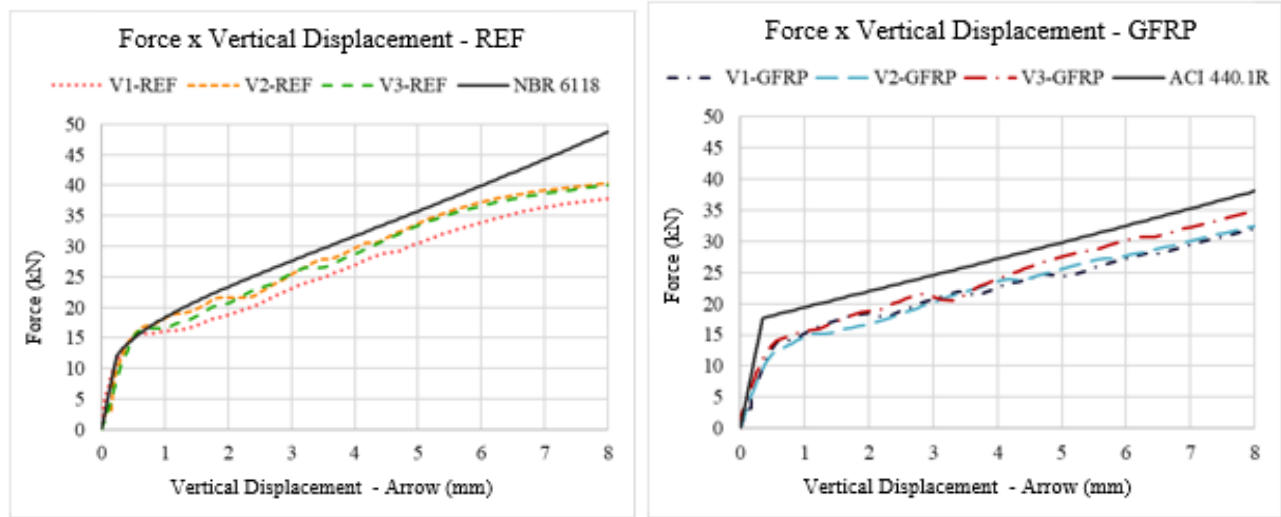


Figure 16. Force vs. experimental and theoretical vertical displacement.

Figure 16 shows the different behaviors between the two predicted deflections and their respective experimental values. By adhering to NBR 6118 (2014), results similar to actual values were obtained, particularly at the moment when the beams cracked and showed behavior changes. However, the analytical shifts of the two sets of simulated values were consistent with the experimental values.

Although the calculated deflections underestimated the experimental values, the actual behavior of the structure depended on a few variables, such as the properties of the materials, which directly affected the analytical results. Therefore, the calculated deflections were less accurate, which rendered it difficult to arrive at conclusions (Filho, 2014).

4. Conclusions and comments

The low modulus of elasticity of GFRP bars directly affected the rigidity of structures, which rendered the latter more susceptible to vertical displacements and crack openings. This characteristic, as predicted by ACI 440.1R-15 (2015), resulted in larger areas of bending reinforcement. In this study, 2,5 times the area of steel was required to maintain a similar behavior. In highly aggressive environments, similar reinforcement coverage is recommended by the regulations of both groups.

The sizing of the GFRP-reinforced beams should only be performed after verifying the SLS for excessive deformation, as their final resistance to bending can exceed this limit by approximately 160%. This remaining strength offers structural safety and signaling.

A distinction was observed between the specific deformations of the bars. The GFRP bars showed less deformation than the steel bars and exhibited linearity until failure because they did not flow. After loading was terminated, the GFRP bar returned to its undeformed state, which confirmed its elastic behavior.

Two of the three GFRP beams did not satisfy the SLS-DEF at the desired bending moment, which indicates an underestimation of the forecast by ACI 440.1R-15 (ACI, 2015). Based on a comparison of the analytical forecasts and experimental results, ACI 440.1R-15 (2015) predicted the maximum bending strength of the beam with higher precision, whereas NBR 6118 (2014) provided more conservative forecasts. Although the GFRP beams supported lower loads and exhibited greater deformations within the SLS-DEF when compared to the steel-reinforced beams, they were able to perform structural functions safely.

Author contributions: Cristian Espíndola Farias (Conceptualization, Data Curation, Formal analysis, Investigation, and Methodology), Sarah Lodeti Pessi (Resources, Review & Editing, and Investigation), Augusto Wanderlind (Resources,

Supervision, Writing, and Review & Editing), Jorge Henrique Piva (Resources, Supervision, Writing, and Review & Editing), Elaine Guglielmi Pavei Antunes (Conceptualization, Investigation, Methodology, Resources, Supervision, and Writing - Review & Editing).

Financial support: STRATUS Compositos Estrutural LTDA donated the GFRP rebars used in the current study.

Conflicts of interest: The authors declare no conflicts of interest.

Acknowledgments: We would like to thank Editage (www.editage.com) for English language editing.

References

- Abdelkarim, O. I., Ahmed, E. A., Mohamed, H. M., & Benmokrane, B. (2019). Flexural strength and serviceability evaluation of concrete beams reinforced with deformed GFRP bars. *Engineering Structures*, 186, 282–296. <https://doi.org/10.1016/j.engstruct.2019.02.024>
- ABNT. (2003). NBR NM 248: Agregados - Determinação da composição granulométrica. Associação brasileira de normas técnicas.
- ABNT. (2014). NBR 6118: Projeto de estruturas de concreto – Procedimento. Associação brasileira de normas técnicas. Rio de Janeiro, Brazil.
- ABNT. (2015). NBR 5738: Concreto - Procedimento para moldagem e cura de corpos de prova. Associação brasileira de normas técnicas. Rio de Janeiro, Brazil.
- ABNT. (2018). NBR 5739: Concreto – Ensaio de compressão de corpos-de-prova cilíndricos. Associação brasileira de normas técnicas. Rio de Janeiro, Brazil.
- ACI (American Concrete Institute). (2008). Specification for Construction with Fiber-Reinforced Polymer Reinforcing Bars. ACI 440.5-08, Farmington Hills, MI.
- ACI (American Concrete Institute). (2015). Guide for the Design and Construction of Structural Concrete Reinforced with Fiber-Reinforced Polymer (FRP) Bars. ACI 440.1R-15, Farmington Hills, MI, 88.
- Ascione, L., Mancusi, G., & Spadea, S. (2010). Flexural behaviour of concrete beams reinforced with GFRP bars. *Strain*, 46(5), 460–469. <https://doi.org/10.1111/j.1475-1305.2009.00662.x>
- ASTM (American Society for testing and materials). (2018). Standard Test Method for Flexural Strength of Concrete (Using Simple Beam with Third-Point Loading). ASTM C78/C78M - 18, Pensilvânia.
- Confrere, A., Michel, L., Ferrier, E., & Chanvillard, G. (2016). Experimental behaviour and deflection of low-strength concrete beams reinforced with FRP bars. *Structural Concrete*, 17(5), 858–874. <https://doi.org/10.1002/suco.201500046>
- CSA S806. (2012). Design and construction of building structures with fibre-reinforced polymers. Canadian Standards Association (CSA) Standard S806-12.
- El-Nemr, A., Ahmed, E. A., El-Safty, A., & Benmokrane, B. (2018). Evaluation of the flexural strength and serviceability of concrete beams reinforced with different types of GFRP bars. *Engineering Structures*, 173, 606–619. <https://doi.org/10.1016/j.engstruct.2018.06.089>
- Fava, G., Carvelli, V., & Pisani, M. A. (2016). Remarks on bond of GFRP rebars and concrete. *Composites Part B: Engineering*, 93, 210–220. <https://doi.org/10.1016/j.compositesb.2016.03.012>
- Filho, R. C. C. and J. R. F. (2014). Cálculo e Detalhamento de Estruturas Usuais de Concreto Armado: segundo a NBR 6118:2014. (4), São Carlos.
- I. S. Hoffman and E. G. P. Antunes. (2017). Análise experimental de vigas mistas de concreto armado e perfis de gfrp utilizados como substitutos parciais das armaduras transversais. T.C.C. Dept. Civil. Eng., Universidade do Extremo Sul Catarinense, Criciúma, 25f.
- Jabbar, S. A. A., & Farid, S. B. H. (2018). Replacement of steel rebars by GFRP rebars in the concrete structures. *Karbala International Journal of Modern Science*, 4(2), 216–227. <https://doi.org/10.1016/j.kijoms.2018.02.002>
- Ramachandra Murthy, A., Pukazhendhi, D. M., Vishnuvardhan, S., Saravanan, M., & Gandhi, P. (2020). Performance of concrete beams reinforced with GFRP bars under monotonic loading. *Structures*, 27, 1274–1288. <https://doi.org/10.1016/j.istruc.2020.07.020>
- Saleh, Z., Goldston, M., Remennikov, A. M., & Sheikh, M. N. (2019). Flexural design of GFRP bar reinforced concrete beams: An appraisal of code recommendations. *Journal of Building Engineering*, 25. <https://doi.org/10.1016/j.job.2019.100794>
- Sheikh, S. A., & Kharal, Z. (2018). Replacement of steel with GFRP for sustainable reinforced concrete. *Construction and Building Materials*, 160, 767–774. <https://doi.org/10.1016/j.conbuildmat.2017.12.141>
- Tavares, D. H., & Giongo, J. S. (2009). Análise teórica e experimental de vigas de concreto armadas com barras não metálicas de GFRP. *Cadernos de Engenharia de Estruturas*, 11(52), 143–156.

- Umair-Saleem, M., Khurram, N., Nasir-Amin, M., & Khan, K. (2018). Finite element simulation of RC beams under flexure strengthened with different layouts of externally bonded fiber reinforced polymer (FRP) sheets. *Revista de La Construcción*, 17(3), 383–400. <https://doi.org/10.7764/rdlc.17.3.383>
- Yoo, D. Y., Banthia, N., & Yoon, Y. S. (2016a). Flexural behavior of ultra-high-performance fiber-reinforced concrete beams reinforced with GFRP and steel rebars. *Engineering Structures*, 111, 246–262. <https://doi.org/10.1016/j.engstruct.2015.12.003>
- Yoo, D. Y., Banthia, N., & Yoon, Y. S. (2016b). Predicting service deflection of ultra-high-performance fiber-reinforced concrete beams reinforced with GFRP bars. *Composites Part B: Engineering*, 99, 381–397. <https://doi.org/10.1016/j.compositesb.2016.06.013>